

HIGH-VOLTAGE GAIN DC-DC CONVERTER FOR PHOTOVOLTAIC APPLICATIONS IN DC NANOGIDS

Yury Pontes¹, Carlos Elmano de A. e Silva², Edilson Mineiro Sá Jr.³

¹Federal university of Ceará (UFC), Sobral –CE, Brazil

²Federal university of Ceará (UFC, Sobral –CE, Brazil

³Federal Institute of Education, Science and Technology (IFCE), Sobral –CE, Brazil

e-mail: yuryeletrica@hotmail.com, carloselmano@gmail.com edilson.mineiro@gmail.com

Abstract – Photovoltaic (PV) systems used in DC Nanogrids present prominent advantages associated with low maintenance need and operation costs. Owing to the low output voltage of the PV module, highly efficient high-voltage gain DC-DC converters are required for connection with the DC nanogrid. This work presents a novel DC-DC converter topology with current source characteristic for PV applications and current injection in DC nanogrids. The introduced converter uses coupled inductors and switched capacitors to achieve high voltage gain with low component count and without using extreme duty ratios. Besides, the main switch is turned on with nearly zero current, thus contributing to minimized switching losses. The qualitative and quantitative analyzes of the circuit are presented in detail and a prototype rated at 200 W is developed and evaluated in the laboratory. Experimental results demonstrate efficient renewable energy conversion, where the maximum efficiency is 96.8%.

Keywords – DC Nanogrids, Grid connected, High Step-up DC-DC converter, High voltage gain, Photovoltaic (PV).

I. INTRODUCTION

The continuous evolution of semiconductor technology has allowed the improved use of DC distribution systems [1]–[7], with consequent increase of efficiency due to the lack of ac-DC converters typically required to provide power factor correction [5].

By definition, a DC nanogrid is a DC distribution system where one or more DC energy sources, e.g., photovoltaic modules, fuel cells, DC generators, among others, provide power to a DC bus in low power plants [8], [9].

A DC nanogrid can operate in standalone mode or connected to a local power grid. It is also possible to distribute energy through an ac bus, i.e., ac nanogrid, or using a hybrid approach [10]–[14].

Since most renewable energy sources operate with DC quantities, as well as energy storage devices (ESDs) and often electronic loads, DC nanogrids become more efficient, due to less energy conversion stages [5], with prominent advantages over their ac counterparts [15]–[18].

The use of photovoltaic (PV) systems in DC nanogrids is quite attractive due to the low maintenance and operating [9]. In this context, DC buses rated at 380 V are widely employed in several applications [19]–[21]. Since the PV modules typically provide low voltages rated between 20 V and 50 V, the series connection of PV modules is employed to obtain higher voltages, which allows the use of basic DC-DC converters in the interconnection between PV modules and the DC bus [22]. In such conditions, partial or total shading can compromise the operation at the maximum power point (MPP) [23]. Therefore, the use of high-voltage gain DC-DC converters is an alternative, since it allows the individual tracking of the MPP in each module, thus optimizing the extraction of power and bringing system modularity.

Several high-voltage gain DC-DC converter topologies have been proposed so far in the literature [8], [9], [24]–[32]. Among the existing approaches the extend conversion range, cascaded converters, voltage multipliers, multilevel converters, interleaved converters, switched capacitors and coupled inductors can be highlighted [33]–[35]. The use of coupled inductors has drawn significant attention, since it allows obtaining a high static gain while using few components in the power circuit. However, if the turns ratio is high, the voltage across the output diode will also be. In addition, resonance between the leakage inductance and the intrinsic capacitance of the output diode may cause overvoltage on the active switch, thus leading to the need of clamping circuits [36], [37].

A circuit composed of a diode and a capacitor was employed in [36] to provide the active clamping of the voltage across the Metal Oxide Semiconductor Field Effect Transistor (MOSFET), as the energy associated with the leakage inductance can be absorbed. A family of high-voltage gain converters based on coupled inductors and distinct configurations for the clamping capacitor was introduced in [37]. Besides, the leakage inductance is used to control the falling rate of the current through the output diode, thus minimizing reverse recovery issues. The use of clamping capacitors associated with distinct positions in a coupled-inductor-based boost converter was also analyzed in [38], as the voltage stresses on the capacitors are minimized without changing the operating principle of the converter.

Most high-voltage gain converters described in the literature have an output with voltage source characteristic.

Manuscript received 04/06/2020; first revision 07/16/2020; accepted for publication 11/09/2020, by recommendation of Editor Demercil de Souza Oliveira Jr. ” <http://dx.doi.org/10.18618/REP.2020.4.0021>

Therefore, an eventual voltage disturbance in the DC bus can cause current peaks in the output of the converter and reduce the life of the capacitors [39]. In addition, devices connected to the same bus operating at different frequencies may cause beat frequency oscillations [39]. In this context, DC-DC converters with current source characteristic at the output has the output current limited by output inductor, allowing the converter to be connected to a voltage bus without generating current peaks and oscillations that can cause instability.

This work proposed a non-isolated DC-DC conversion for high-voltage step-up for PV system applications and current injection in DC nanogrids. The main advantages lie in low component count and use of the leakage inductance associated with the coupled inductors to provide nearly zero current switching (ZCS), leading to minimized switching losses. The stores energy is then recovered, thus avoiding high voltage spikes on the switch and increasing the converter efficiency.

II. CONVERTER ANALYSIS

A. Circuit Description

The proposed converter is shown in Fig. 1. The coupled inductances L_p e L_s are replaced by the simplified model of a transformer in Fig. 3 (a), which allows analyzing the influence of the leakage inductances. The number of turns of the primary and secondary windings in the ideal transformer are given by N_1 and N_2 , respectively. The magnetizing inductance of the transformer corresponds to L_m , while the leakage inductances are L_{KP} and L_{KS} . The circuit composed of capacitor C_3 and diode D_2 clamp the voltage across the main switch S_1 , thus absorbing the energy stored in L_{KP} and allowing the use of switches with lower rated voltages and consequently reduced conduction losses. The switched capacitors C_1 and C_2 provide higher voltage gain to the converter and damp the resonance associated with the leakage inductances and the intrinsic capacitances of diodes D_1 and D_2 . The switching frequency of S_1 is f_s . The output side of the converter have current source characteristic provided by L_o in series with the output stage represented by a constant voltage V_o . The converter operates in continuous conduction mode (CCM) since the current through the magnetizing inductance L_M does not become null over the switching period. The main theoretical waveforms are presented in Fig. 2, while the operation modes are detailed in Fig. 3.

B. Operation Stages

In order to perform the qualitative analysis, capacitances C_1 , C_2 , and C_3 are considered large enough so that their respective voltages are constant with negligible ripple. All semiconductors are considered to be ideal and the converter operates in CCM according to Fig. 3.

Mode 1 ($t_0 - t_1$): Switch S_1 is turned on under nearly ZCS condition. The current through D_1 decreases as limited by L_{KS} , being the diode reverse biased at t_1 with zero current. Inductors L_m and L_{KP} store the energy supplied by V_{IN} . Diodes D_2 and D_3 remain reverse biased. Capacitors C_1 , C_2 , and C_3 provide energy to L_o and V_o . This mode finishes when the current through D_1 becomes null.

Mode 2 ($t_1 - t_2$): Diodes D_1 and D_2 are reverse biased at t_1 , while both S_1 and D_3 are on. Due to the magnetic coupling, the magnetizing inductance is responsible for charging C_2 , whose voltage depends on the turns ratio between N_1 and N_2 . Inductances L_m , L_{KP} , L_{KS} , and L_o store energy. Capacitors C_1 , C_2 , and C_3 provide energy to the DC bus of the nanogrid. This mode finishes when S_1 is turned off.

Mode 3 ($t_2 - t_3$): Switch S_1 is turned off at t_2 , while the polarity of the voltage across the inductors is inverted. Diode D_1 is reverse biased. Diode D_2 is forward biased and the energy stored in L_{KP} is transferred to C_3 , as the voltage across the switch is clamped with reduced voltage spikes. The current through D_3 decreases according to a rate defined by L_{KS} , as the diode is turned off under ZCS condition and this mode finishes.

Mode 4 ($t_3 - t_4$): Both S_1 and D_3 are off at t_3 . Diode D_1 is forward biased as the current through it is limited by L_{KS} . Diode D_2 is still forward biased, thus allowing C_3 to be completely charged. Besides, the voltage across C_1 is proportional to the sum of the voltages across the primary and secondary windings. Inductor L_o provides energy to the output stage. This mode finishes when D_2 is reverse biased.

Mode 5 ($t_4 - t_5$): Only diode D_1 remains forward biased. Capacitor C_1 is still charged, while C_2 , C_3 , and L_o provide energy to the output stage. This mode finishes when S_1 is turned on.

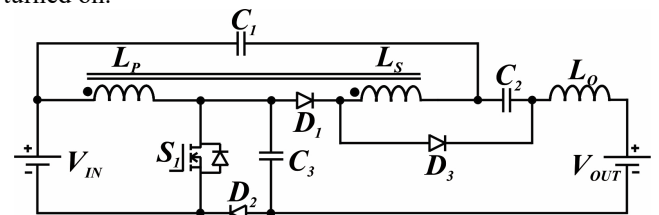


Fig. 1. Proposed coupled inductor based converter.

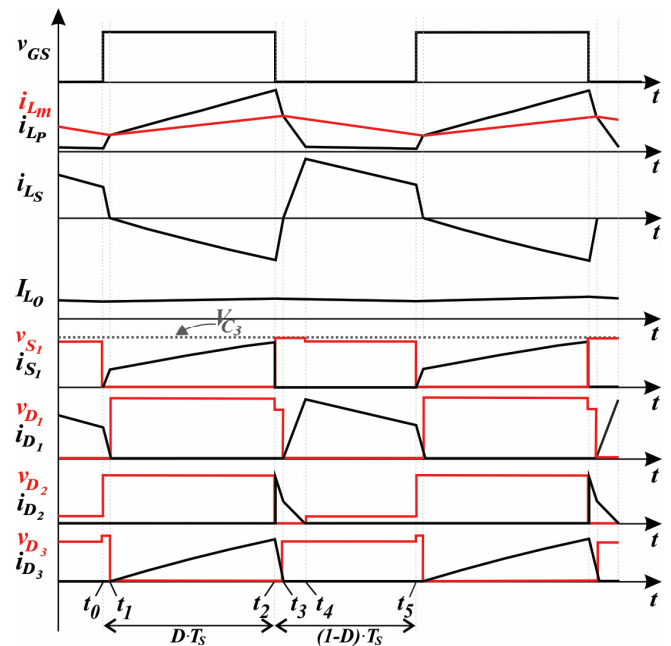


Fig. 2. Main theoretical waveforms of the proposed DC-DC converter.

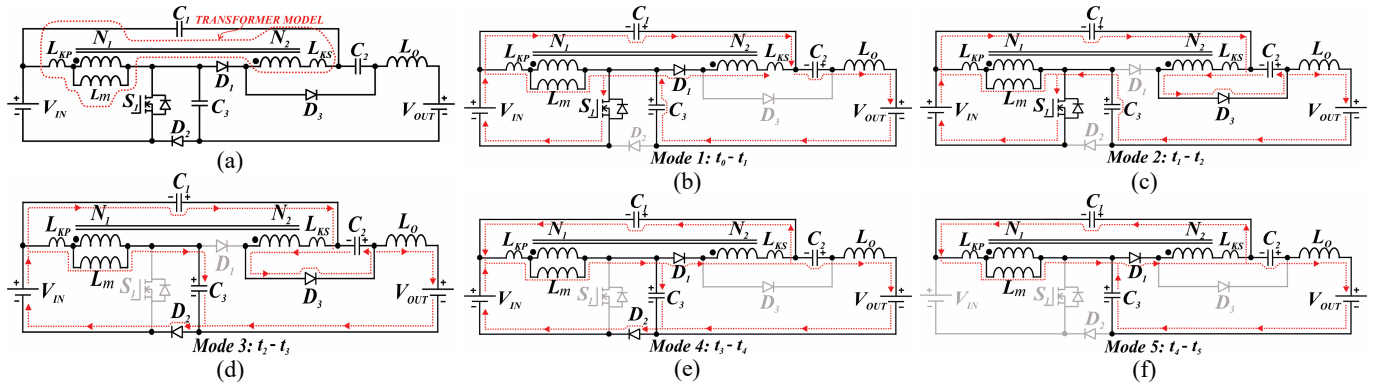


Fig. 3. (a) Circuit employing an ideal transformer model representing the coupled inductors. Operation modes of the proposed DC-DC converter: (b) Mode 1 ($t_0 - t_1$); (c) Mode 2 ($t_1 - t_2$); (d) Mode 3 ($t_2 - t_3$); (e) Mode 4 ($t_3 - t_4$); (f) Mode 5 ($t_4 - t_5$).

C. Static Gain

In order to determine the static gain, switch S_1 is assumed to be on during $D \cdot T_s$ and off during $(1-D) \cdot T_s$, where D is the duty cycle and T_s is the switching period. The turns ratio of the coupled inductors given by n is:

$$n = \frac{N_1}{N_2} \quad (1)$$

where:

N_1 – number of turns of the primary winding;

N_2 – number of turns of the secondary winding.

Some authors only consider the influence of the primary leakage inductance L_{KP} , while neglecting the secondary leakage inductance L_{KS} [26], [40], [41]. It is worth mentioning that L_{KS} is responsible for limiting the di/dt of the current through the active switch, being an important parameter for the circuit analysis. However, in order to simplify the calculations, the secondary leakage inductance L_{KS} influence on static gain can be disconsidering. The coupling factor k can be defined [9]:

$$k = \frac{L_m}{L_m + L_{KP} + \frac{L_{KS}}{n^2}} \quad (2)$$

During the time interval defined by $D \cdot T_s$, the voltage across the magnetizing inductance is:

$$V_{L_m} = \frac{L_m}{L_m + L_{KP}} \cdot V_{IN} = k \cdot V_{IN} \quad (3)$$

where V_{IN} is the average input voltage.

The current through the secondary winding is much lower than that through the primary winding. Thus, the influence of L_{KS} on the charging process of capacitors C_1 and C_2 can be neglected. Then, the voltage across C_2 is:

$$V_{C_2} = k \cdot n \cdot V_{IN} \quad (4)$$

During the time interval defined by $(1-D) \cdot T_s$, the voltage across the magnetizing inductance is:

$$V_{L_m} = k \cdot (V_{C_3} - V_{IN}) \quad (5)$$

Besides, the voltage across secondary winding L_s is equivalent to the reflected voltage V_{L_m} , i.e.:

$$V_{L_s} = k \cdot n \cdot (V_{C_3} - V_{IN}) \quad (6)$$

The average voltage across L_m is null during T_s , resulting in:

$$\int_0^T V_{L_m}(t) dt = \int_0^{DT} V_{L_m}(t) dt + \int_{DT}^T V_{L_m}(t) dt = 0 \quad (7)$$

Substituting (3) and (5) in (7) it is possible to determine the average voltage across C_3 as:

$$V_{C_3} = \frac{1}{1-D} \cdot k \cdot V_{IN} \quad (8)$$

When switch S_1 is ed off, capacitor C_1 is charged with the sum of the voltages across the primary and secondary windings, i.e.:

$$V_{C_1} = k \cdot (V_{C_3} - V_{IN}) + (k \cdot n \cdot (V_{C_3} - V_{IN})) \quad (9)$$

Substituting (8) in (9), it is possible to determine V_{C_1} V_{C_1} :

$$V_{C_1} = \frac{V_{IN} \cdot D}{1-D} \cdot (1+n) \cdot k \quad (10)$$

The average output voltage V_{OUT} corresponds to the sum of the voltages across C_1 , C_2 , and C_3 :

$$V_{OUT} = \left(\frac{V_{IN} \cdot D \cdot (1+n) \cdot k}{1-D} + V_{IN} \cdot n \cdot k + \frac{k \cdot V_{IN}}{1-D} \right) \quad (11)$$

Rearranging (11), the static gain M can be obtained in the form:

$$M = \frac{V_{OUT}}{V_{IN}} = \frac{1 + (D+n) \cdot k}{1-D} \quad (12)$$

Considering the ideal model in Fig. 1 (a), the static gain can be determined for $k=1$ as:

$$M = \frac{V_{OUT}}{V_{IN}} = \frac{1 + D + n}{1-D} \quad (13)$$

The voltage clamping on S_1 is provided by C_3 . Thus, for $k=1$ the voltage across S_1 can be determined substituting (13) in (8):

$$V_{S_1} = V_{C_3} = \frac{V_{IN}}{1-D} = \frac{V_{OUT}}{1 + D + n} \quad (14)$$

Fig. 4 (a) presents a gain curve of the boost converter and the gain static curves of proposed converter for different coupling factor values.

The equations (15), (16), (17) and (18) calculate the minimum value of the capacitors and the output inductor of

the converter. The converter switches were chosen according to the voltage and current efforts.

$$C_1 = \frac{I_o \cdot (1-D)}{f_s \cdot \Delta V_C \cdot V_{IN} \cdot D \cdot (1+n)} \quad (15)$$

$$C_2 = \frac{I_o}{f_s \cdot \Delta V_C \cdot n \cdot V_{IN}} \quad (16)$$

$$C_3 = \frac{I_o \cdot (1-D)}{f_s \cdot \Delta V_C \cdot V_{IN}} \quad (17)$$

$$L_o = \frac{V_{IN} \cdot D^2}{(1-D) f_s \cdot \Delta I_{L_o}} \quad (18)$$

where:

ΔV_C – Maximum percentage voltage ripple in the capacitors;

ΔI_{L_o} – Maximum percentage current ripple in the inductor L_o .

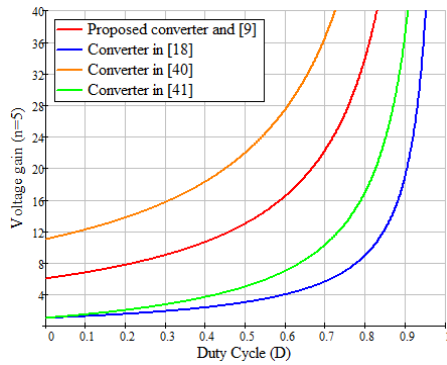


Fig. 4. Ideal static gain curves of the proposed converter and of the converters presented in table II.

TABLE I

PROTOTYPE COMPONENTS SPECIFICATIONS

Parameter	Specifications
S_1	IRFB4310 (International Rectifier)
$D_1 = D_3$	IDT02S60C (Infineon)
D_2	STPS3150 (STMicroelectronics)
$C_1 = C_2$	2 μ F/400V (MKP-379 Vishay)
C_3	4 x (10 μ F/100V) Multilayer Ceramic – MLCC – SMD/X7R/12105C106KAT2A AVX/Kyocera
L_o	5 mH -NEE – MTT140EE3007 Magmattec Core: MTT140EE4012 Magmattec
L_p / L_s	$N_1:N_2 = 11:55/L_p = 52\mu\text{H}/L_s = 1.4 \text{ mH}$ $L_{KP} = 657\text{nH}/k = 0.987$

D. Comparison among the proposed converter and other similar DC-DC topologies

Table II presents a comparison of the proposed converter with the topologies presented in [9], [18], [40], [41]. Some criteria were considered to select the converters in table II: drive complexity, number of components, photovoltaic applications, high voltage gain and high efficiency. The converter introduced in [9] has current source characteristic at the output. However, it uses an extra diode and capacitor, what may lead to reduced efficiency. The converter proposed in [18] employs few components, but three active switches are necessary, with consequent increase of complexity associated with the drive circuitry. Besides, the output presents voltage source characteristic. A DC-DC interface converter for DC microgrids is described in [40], whose output behaves as a voltage source. Besides, an auxiliary clamping circuit is required to limit the maximum voltage across the switch, while complexity is increased as a consequence. The high-voltage gain DC-DC converter proposed in [41] presents high efficiency, but the output has voltage source characteristic. Two active switches are also employed in the power stage, resulting in increased cost and reduced robustness. The converter proposed in this manuscript has few components, only one switch which reduces the complexity of activation and output with a current source characteristic which helps in reducing problems associated with the beat frequency [39].

The photovoltaic modules have parasitic capacitances distributed throughout the panel, intrinsic to the manufacture. In the presence of voltage at the terminals of the panel, the load stored by these capacitances can flow through the common point of the system, generating a leakage current that will circulate between the panel and the network. Without galvanic isolation or a common mode filter, the leakage current can be large enough to activate the inverter protection system, removing it from the grid, for example [43], [44]. These currents can cause electromagnetic interference, harmonics in the electrical network and losses in the circuit. In this converter, the L_o output inductor can be bypassed to form a common mode filter without changing the converter's operating modes. However, to simplify the operation analysis of the converter, the prototype was developed disregarding the common mode configuration of the inductor.

TABLE II

COMPARISON AMONG THE CONVERTERS PRESENTED IN [9], [18], [40], AND [41] AND THE PROPOSED TOPOLOGY.

Parameter	Topologies				
	Converter in [9]	Converter in [18]	Converter in [40]	Converter in [41]	Proposed converter
Diodes	4	2	4	2	3
Switch	1	3	2	2	1
Capacitor	4	1	5	3	3
Coupled Inductor	1	0	1	0	1
Inductor	1	2	0	3	1
Voltage Gain	$\frac{1+D+n}{1-D}$	$\frac{1+D1}{1-D1-D2}$	$\frac{1+2n}{1-D}$	$\frac{3D+1}{1-D}$	$\frac{1+D+n}{1-D}$
Voltage stress of main switch	$\frac{V_{OUT}}{1+D+n}$	$\frac{V_{OUT}+V_{IN}}{2}$	$\frac{V_{OUT}}{1+2n}$	$\frac{V_{OUT}}{1+3D}$	$\frac{V_{OUT}}{1+D+n}$
Output characteristic	current source	voltage source	voltage source	voltage source	current source
Total number of components	11	8	12	10	9

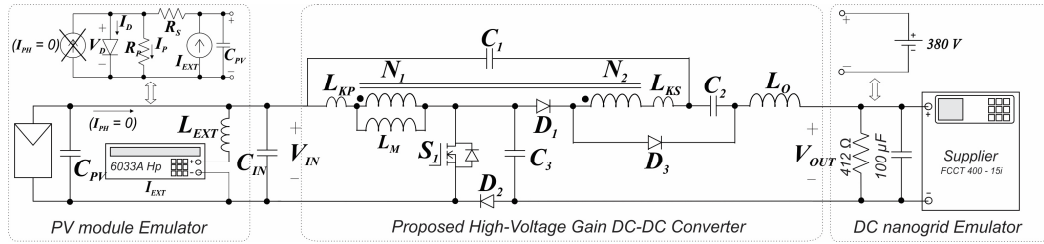


Fig. 5. Laboratory setup using the method proposed in [42], where an external current source is connected to the input to emulate the photogenerated current. A voltage source is used at the output to emulate DC bus of the nanogrid.

III. EXPERIMENTAL VALIDANTION

In order to validate the theoretical assumptions and evaluate the performance of the proposed converter, a 200-W prototype was implemented in the laboratory, being connected to PV module KD210GX-LPU by Kyocera under the manufacturer's standard test conditions. Table I summarizes the components used in the prototype, while Fig. 5 presents the experimental setup employed in the tests. The method proposed in [42] was adopted to evaluate the converter in the laboratory, where a PV module emulator is required.

The detailed setup is represented in Fig. 5. A programmable source model 6033A by HP is configured to operate as a current source. A voltage source model FCCT400 – 15i by Supplier was adjusted to provide a DC voltage of 380 V aiming to emulate the DC nanogrid. This power supply not absorb power. Thus, a 412 Ω interface resistor is added to the output terminals to guarantee the power flux direction of converter to load. The converter was designed with an input voltage of 26 V while operating at 50 kHz. The output voltage and output current are shown Fig. 6 (a). The voltages across C_1 , C_2 , and C_3 , and the voltage clamping as provided by C_3 can be seen in Figs. 6 (b) and 6 (c), respectively. Fig. 6 (d) shows the voltage and current waveforms in the active switch, while the detailed view in Fig. 6 (e) denotes low switching losses during turn on. As expected, the maximum voltage across S_1 is about 60 V. The currents through the primary inductance (I_{Lp}), secondary inductance (I_{Ls}), and magnetizing inductance (I_{Lm}) are represented in Fig. 6 (f). The commutation of diodes D_1 , D_2 , and D_3 is shown in Figs. 6 (g), 6 (i), and 6 (k), respectively. The detailed views presented in Figs. 6 (h), 6 (j), and 6 (l) clearly evidence that such diodes are turned off under ZCS condition, thus contributing to the minimization of switching losses. The efficiency curve of the converter as a function of the output power for $V_{IN}=26$ V is presented in Fig. 7, being measured with power analyzer PA4000 by Tektronix. Since the converter designed for PV applications, EURO (European Efficiency) and the CEC (California Energy Commission) standards were adopted [8], [9], resulting in:

$$\eta_{EURO} = (0.03 \cdot 95.4) + (0.06 \cdot 96.08) + (0.13 \cdot 96.57) + (0.1 \cdot 96.65) + (0.48 \cdot 96.8) + (0.2 \cdot 95.4) = 96.38\% \quad (19)$$

$$\eta_{CEC} = (0.04 \cdot 96.08) + (0.05 \cdot 96.57) + (0.12 \cdot 96.65) + (0.21 \cdot 96.8) + (0.53 \cdot 96.3) + (0.05 \cdot 95.4) = 96,4\% \quad (20)$$

Analogously to the proposed converter, the topology in [9] has output current source characteristic and presents a

maximum efficiency of 94.7%. Considering standards EURO and CEC, the efficiencies become 96.38% and 96.4%, respectively. Fig. 8 shows the distribution of losses among the power stage components, being D_2 the major responsible for the existing losses due high current conduction. A picture of the laboratory prototype is represented in Fig. 9, where capacitor C_3 is assembled at the bottom layer of the printed circuit board (PCB).

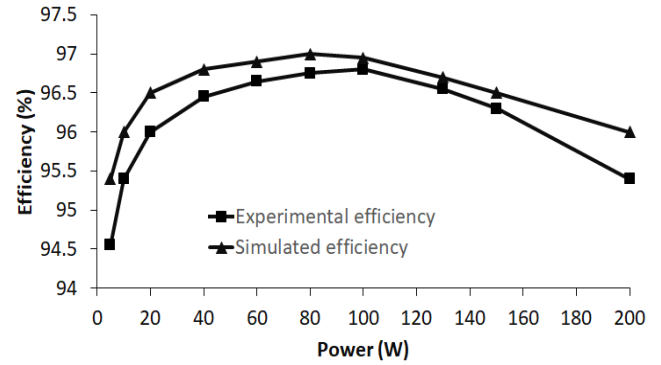


Fig. 7. Efficiency curve of proposed converter for $V_{IN}=26$ V.

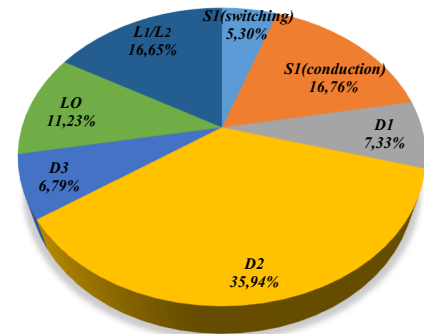


Fig. 8. Percent distribution of losses in the power stage components at the rated power condition.

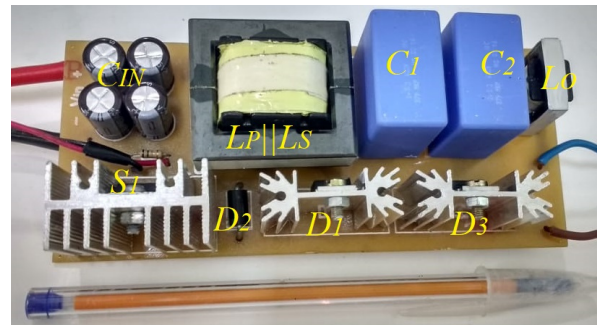


Fig. 9. Laboratory prototype.

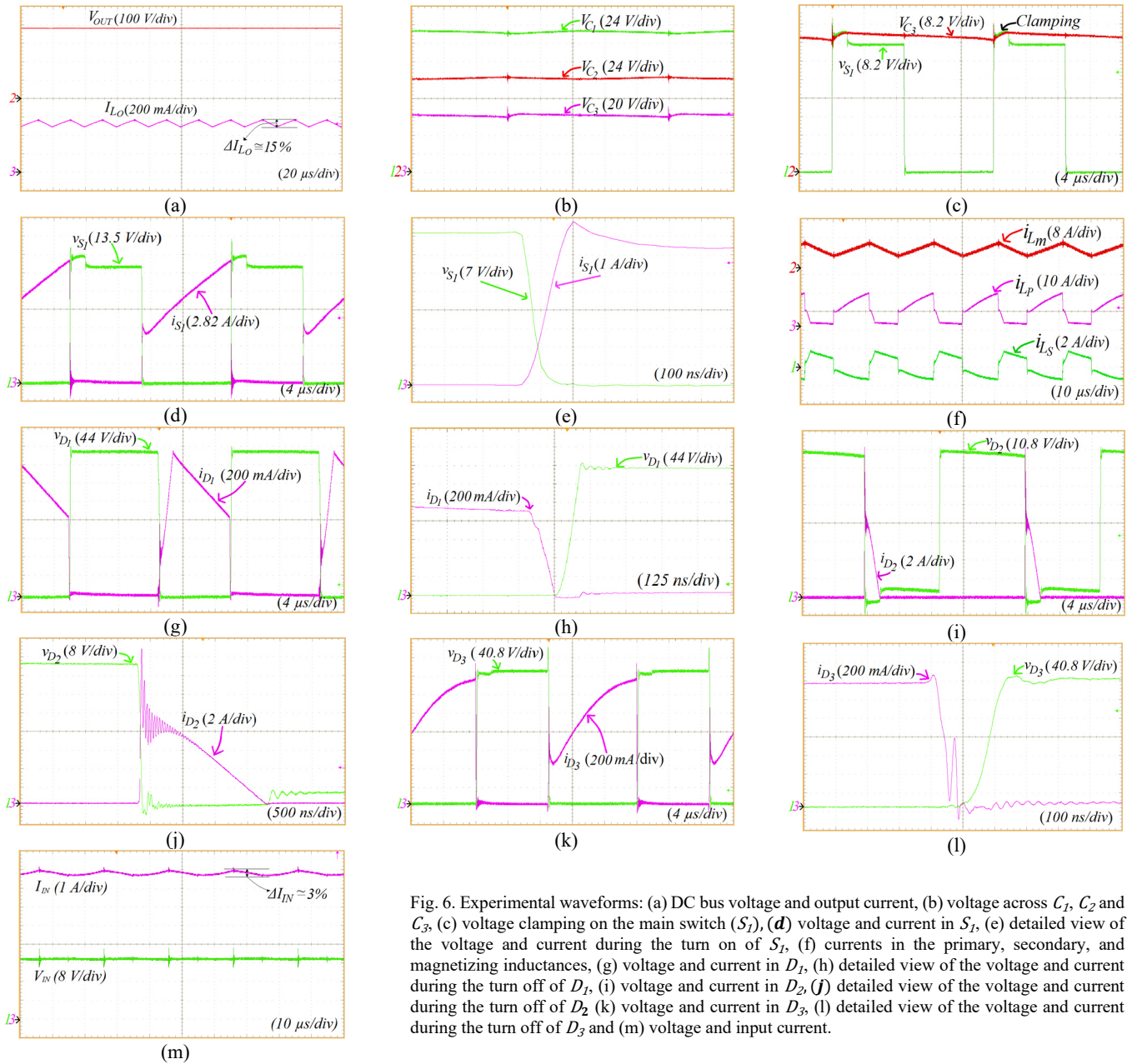


Fig. 6. Experimental waveforms: (a) DC bus voltage and output current, (b) voltage across C_1 , C_2 and C_3 , (c) voltage clamping on the main switch (S_1), (d) voltage and current in S_1 , (e) detailed view of the voltage and current during the turn on of S_1 , (f) currents in the primary, secondary, and magnetizing inductances, (g) voltage and current in D_1 , (h) detailed view of the voltage and current during the turn off of D_1 , (i) voltage and current in D_2 , (j) detailed view of the voltage and current during the turn off of D_2 , (k) voltage and current in D_3 , (l) detailed view of the voltage and current during the turn off of D_3 and (m) voltage and input current.

IV. CONCLUSIONS

This paper has proposed a non-isolated DC-DC converter with high-voltage gain and output current source characteristic for PV system applications and current injection in DC nanogrids. The qualitative and quantitative analyses of the topology were derived, as prominent advantages over existing approaches can be clearly evidenced, e.g., high-voltage gain with low component count, use of a single active switch with regenerative clamping, and high efficiency over a wide load range. The clamping circuit is responsible for absorbing the energy stored in the leakage inductance, thus leading to reduced voltage stresses on the active switch and minimized losses during turn on as demonstrated by the experimental waveforms. Besides, it is possible to use MOSFETs with low $R_{DS(on)}$, what also contributes to reduction of cost and conduction losses. The diode losses are also typically low because soft switching is achieved during turn off. The experimental results validated the proposed converter. The

maximum efficiency measured in the prototype is 96.8%, while the efficiencies considering EURO and CEC standards are 96.38% and 96.4%, respectively.

REFERENCES

- [1] A. Sannino, G. Postiglione, M. H. J. Bollen, and S. Member, "Pterygonema_alatum.pdf," vol. 39, no. 5, pp. 1499–1507, 2003.
- [2] S. I. Ganesan, D. Pattabiraman, R. K. Govindarajan, M. Rajan, and C. Nagamani, "Control Scheme for a Bidirectional Converter in a Self-Sustaining Low-Voltage DC Nanogrid," *IEEE Trans. Ind. Electron.*, vol. 62, no. 10, pp. 6317–6326, 2015.
- [3] D. Salomonsson and A. Sannino, "Load modelling for steady-state and transient analysis of low-voltage DC systems," *IET Electr. Power Appl.*, vol. 1, no. 5, p. 690, 2007.
- [4] A. T. Elsayed, A. A. Mohamed, and O. A. Mohammed,

- “DC microgrids and distribution systems: An overview,” *Electr. Power Syst. Res.*, vol. 119, pp. 407–417, 2015.
- [5] D. Burmester, R. Rayudu, W. Seah, and D. Akinyele, “A review of nanogrid topologies and technologies,” *Renew. Sustain. Energy Rev.*, vol. 67, pp. 760–775, 2017.
- [6] T. F. Wu, Y. K. Chen, G. R. Yu, and Y. C. Chang, “Design and development of dc-distributed system with grid connection for residential applications,” *8th Int. Conf. Power Electron. - ECCE Asia "Green World with Power Electron. ICPE 2011-ECCE Asia*, pp. 235–241, 2011.
- [7] D. Email, “Intelligent DC Microgrid Living Laboratories - A Sino-Danish Collaboration,” pp. 365–370, 2015.
- [8] M. D. O. Vasconcelos, F. C. De Araújo, F. A. P. Aragão, K. C. A. De Souza, and E. M. Sá, “High static gain DC-DC converter CUK with current source characteristic for nanogrid application,” *2017 IEEE 8th Int. Symp. Power Electron. Distrib. Gener. Syst. PEDG 2017*, pp. 1–6, 2017.
- [9] F. C. De Araújo, M. O. Vasconcelos, F. A. P. Aragão, K. C. A. De Souza, and E. M. Sá, “High-gain DC-DC converter with current source characteristics at the output for applications in photovoltaic systems and current injection in nanogrids,” *2017 IEEE 8th Int. Symp. Power Electron. Distrib. Gener. Syst. PEDG 2017*, pp. 2–7, 2017.
- [10] S. Ahmadi, H. Bevrani, S. Shokoohi, and E. Hasanii, “An improved droop control for simultaneous voltage and frequency regulation in an AC microgrid using fuzzy logic,” in *2015 23rd Iranian Conference on Electrical Engineering*, 2015, vol. 10, pp. 1486–1491.
- [11] A. A. Abdelsalam, H. A. Gabbar, and A. M. Sharaf, “Performance enhancement of hybrid AC/DC microgrid based D-FACTS,” *Int. J. Electr. Power Energy Syst.*, vol. 63, pp. 382–393, 2014.
- [12] A. A. Memon and K. Kauhaniemi, “A critical review of AC Microgrid protection issues and available solutions,” *Electr. Power Syst. Res.*, vol. 129, pp. 23–31, 2015.
- [13] M. Sechilariu, B. C. Wang, F. Locment, and A. Jouglet, “DC microgrid power flow optimization by multi-layer supervision control. Design and experimental validation,” *Energy Convers. Manag.*, vol. 82, pp. 1–10, 2014.
- [14] W. W. Weaver, R. D. Robinett, G. G. Parker, and D. G. Wilson, “Distributed control and energy storage requirements of networked Dc microgrids,” *Control Eng. Pract.*, vol. 44, pp. 10–19, 2015.
- [15] S. S. Nag, R. Adda, O. Ray, and S. K. Mishra, “Current-Fed Switched Inverter based hybrid topology for DC Nanogrid application,” *IECON Proc. (Industrial Electron. Conf.)*, pp. 7146–7151, 2013.
- [16] V. Sudev and S. Parvathy, “Switched boost inverter based Dc nanogrid with battery and bi-directional converter,” *2014 Int. Conf. Circuits, Power Comput. Technol. [ICCPCT-2014]*, pp. 461–467, 2014.
- [17] U. B. Mujumdar and D. R. Tutkane, “Parallel MPPT for PV based residential DC Nanogrid,” in *2015 International Conference on Industrial Instrumentation and Control (ICIC)*, 2015, vol. 54, no. 1, pp. 1350–1355.
- [18] M. Lakshmi and S. Hemamalini, “Nonisolated high gain DC-DC converter for DC microgrids,” *IEEE Trans. Ind. Electron.*, vol. 65, no. 2, pp. 1205–1212, 2018.
- [19] Q. Zhao, F. Tao, and F. C. Lee, “A front-end DC/DC converter for network server applications,” *PESC Rec. - IEEE Annu. Power Electron. Spec. Conf.*, vol. 3, pp. 1535–1539, 2001.
- [20] D. Dong, D. Boroyevich, R. Wang, and I. Cvetkovic, “A two-stage high power density single-phase ac-dc bi-directional PWM converter for renewable energy systems,” *2010 IEEE Energy Convers. Congr. Expo. ECCE 2010 - Proc.*, pp. 3862–3869, 2010.
- [21] W. W. A. G. Silva, P. F. Donoso-Garcia, S. I. Seleme, T. R. Oliveira, C. H. G. Santos, and A. S. Bolzon, “Study of the application of bidirectional dual active bridge converters in dc nanogrid energy storage systems,” *2013 Brazilian Power Electron. Conf. COBEP 2013 - Proc.*, pp. 609–614, 2013.
- [22] W. Li and X. He, “Review of nonisolated high-step-up DC/DC converters in photovoltaic grid-connected applications,” *IEEE Trans. Ind. Electron.*, vol. 58, no. 4, pp. 1239–1250, 2011.
- [23] M. Kasper, D. Bortis, and J. W. Kolar, “Classification and Comparative Evaluation of PV Panel-Integrated DC/DC Converter Concepts,” *IEEE Trans. Power Electron.*, vol. 29, no. 5, pp. 2511–2526, 2014.
- [24] C. Knaesel, L. Michels, A. L. Batschauer, C. Knaesel, L. Michels, and A. L. Batschauer, “FOTOVOLTAICOS High Voltage Gain Isolated INTEGRAÇÃO DC-DC Converter for Integration in Photovoltaic Modules,” pp. 482–493, 2019.
- [25] S. Saravanan and N. Ramesh Babu, “Analysis and implementation of high step-up DC-DC converter for PV based grid application,” *Appl. Energy*, vol. 190, pp. 64–72, 2017.
- [26] M. Muhammad, M. Armstrong, and M. A. Elgendy, “Analysis and implementation of high-gain non-isolated DC–DC boost converter,” *IET Power Electron.*, vol. 10, no. 11, pp. 1241–1249, 2017.
- [27] M. Kumar, M. Ashirvad, and Y. N. Babu, “An integrated Boost-Sepic-Ćuk DC-DC converter with high voltage ratio and reduced input current ripple,” *Energy Procedia*, vol. 117, pp. 984–990, 2017.
- [28] S. Salehi Dobakhshari, J. Milimonfared, M. Taheri, and H. Moradisizkoohi, “A Quasi-Resonant Current-Fed Converter with Minimum Switching Losses,” *IEEE Trans. Power Electron.*, vol. 32, no. 1, pp. 353–362, 2017.
- [29] Y. P. Siwakoti, F. Blaabjerg, and P. C. Loh, “Ultra-step-up DC-DC converter with integrated autotransformer and coupled inductor,” *Conf. Proc. - IEEE Appl. Power Electron. Conf. Expo. - APEC*, vol. 2016-May, no. 1, pp. 1872–1877, 2016.
- [30] Y. P. Siwakoti and F. Blaabjerg, “Single Switch Nonisolated Ultra-Step-Up DC-DC Converter with an Integrated Coupled Inductor for High Boost Applications,” *IEEE Trans. Power Electron.*, vol. 32, no. 11, pp. 8544–8558, 2017.
- [31] A. M. S. S. Andrade, L. Schuch, and M. L. Da Silva Martins, “Analysis and design of high-efficiency hybrid high step-Up DC-DC converter for distributed PV

- generation systems,” *IEEE Trans. Ind. Electron.*, vol. 66, no. 5, pp. 3860–3868, 2019.
- [32] Y. Wang, Y. Qiu, Q. Bian, Y. Guan, and D. Xu, “A Single Switch Quadratic Boost High Step Up DC-DC Converter,” *IEEE Trans. Ind. Electron.*, vol. 66, no. 6, pp. 4387–4397, 2019.
- [33] M. Forouzesh, Y. P. Siwakoti, S. A. Gorji, F. Blaabjerg, and B. Lehman, “Step-Up DC-DC converters: A comprehensive review of voltage-boosting techniques, topologies, and applications,” *IEEE Trans. Power Electron.*, vol. 32, no. 12, pp. 9143–9178, 2017.
- [34] E. S. Hass, C. B. Nascimento, E. S. Hass, and C. B. Nascimento, “A SIMPLE SELF-CLAMPED HIGH STEP-UP DC-DC CONVERTER EMPLOYING COUPLED INDUCTOR A Simple Self-Clamped High Step-Up DC-Dc Converter Employing Coupled Inductor,” pp. 204–213, 2019.
- [35] L. Schmitz, A. I. Pereira, R. G. A. Cacao, D. C. Martins, and R. F. Coelho, “CONVERSOR CC-CC DE ALTO GANHO BASEADO NO CONVERSOR CUK COM INDUTOR ACOPLADO E MULTIPLICADORES DE TENSÃO,” pp. 267–276, 2019.
- [36] Qun Zhao, Fengfeng Tao, Yongxuan Hu, and F. C. Lee, “Active-clamp DC/DC converters using magnetic switches,” *APEC 2001. Sixt. Annu. IEEE Appl. Power Electron. Conf. Expo. (Cat. No.01CH37181)*, vol. 2, pp. 946–952, 2001.
- [37] Q. Zhao and F. C. Lee, “High-efficiency, high step-up dc-dc converters,” *IEEE Trans. Power Electron.*, vol. 18, no. 1 I, pp. 65–73, 2003.
- [38] D. M. Van De Sype, K. De Gussem, B. Renders, A. P. Van Den Bossche, and J. A. Melkebeek, “A single switch boost converter with a high conversion ratio,” *Conf. Proc. - IEEE Appl. Power Electron. Conf. Expo. - APEC*, vol. 3, pp. 1581–1587, 2005.
- [39] X. Yue, D. Boroyevich, F. C. Lee, F. Chen, R. Burgos, and F. Zhuo, “Beat Frequency Oscillation Analysis for Power Electronic Converters in DC Nanogrid Based on Crossed Frequency Output Impedance Matrix Model,” *IEEE Trans. Power Electron.*, vol. 33, no. 4, pp. 3052–3064, 2018.
- [40] S. Sathyan, H. M. Suryawanshi, B. Singh, C. Chakraborty, V. Verma, and M. S. Ballal, “ZVS-ZCS High Voltage Gain Integrated Boost Converter for DC Microgrid,” *IEEE Trans. Ind. Electron.*, vol. 63, no. 11, pp. 6898–6908, 2016.
- [41] M. Forouzesh, Y. Shen, K. Yari, Y. P. Siwakoti, and F. Blaabjerg, “High-Efficiency High Step-Up DC-DC Converter with Dual Coupled Inductors for Grid-Connected Photovoltaic Systems,” *IEEE Trans. Power Electron.*, vol. 33, no. 7, pp. 5967–5982, 2018.
- [42] S. Qin, K. A. Kim, and R. C. N. Pilawa-Podgurski, “Laboratory emulation of a photovoltaic module for controllable insolation and realistic dynamic performance,” *2013 IEEE Power Energy Conf. Illinois, PECI 2013*, pp. 23–29, 2013.
- [43] F. Chen, R. Burgos, and D. Boroyevich, “A Transformerless Single-Phase Utility Interface Converter to Attenuate Common-Mode Voltage for DC Microgrid,” pp. 157–162, 2017.
- [44] V. D. S. Member, V. John, and S. Member, “A Modified Common-Mode Filter with Enhanced Attenuation Performance in Single-Phase Grid-Tied Solar PV Inverters,” pp. 5–10, 2020.

BIOGRAPHIES

Yury Pontes, born in 07/05/1992 in Fortaleza-CE, is an electrical engineer (2016) from Federal University of Ceará and master (2019) from Federal University of Ceará. He is currently a professor at National Industrial Training Service (SENAI). His areas of interest are: power electronics, electronic control systems and renewable energy.

Carlos Elmano de A. e Silva, Graduated (2004), master's (2007) and doctorate (2012) in Electrical Engineering from the Federal University of Ceará. He is currently professor of undergraduate and master's courses in electrical engineering and computer engineering at UFC - Sobral. Has experience in the area of Electrical Engineering, with an emphasis on power electronics, acting mainly on the following themes: three-phase rectifiers, power factor correction and wind energy conversion systems.

Edilson Mineiro Sá Jr., graduated in engineering electrical Engineering at the Federal University of Ceará (1999), Master in Electrical Engineering from Federal University of Ceará (2004) and doctorate from the Federal University of Santa Catarina (2010). He is currently an effective professor of Federal Institute of Education, Science and Technology Campus Sobral and regular professor of the Postgraduate Program in Electrical and Computer Engineering at Federal University of Ceará, Sobral. His areas of interest are: electronic ballasts, microcontrollers, LEDs for illumination, circuits for factor correction power and photovoltaic systems. He is a member of the Association Brazilian Power Electronics – SOBRAEP